Aalborg Universitet

Hypergeometric resummation of self-consistent sunset diagrams for steady-state electron-boson quantum many-body systems out of equilibrium

Couto, Hector Mera; Pedersen, Thomas Garm; Nikolic, Branislav K.

Hypergeometric resummation of self-consistent sunset diagrams for steady-state electron-boson quantum many-body systems out of equilibrium

Héctor Mera,[1,2,*] Thomas G. Pedersen,[2,3] and Branislav K. Nikolić[1]

[1]*Department of Physics and Astronomy, University of Delaware, Newark, Delaware 19716-2570, USA*
[2]*Department of Physics and Nanotechnology, Aalborg University, DK-9220 Aalborg East, Denmark*
[3]*Center for Nanostructured Graphene (CNG), DK-9220 Aalborg East, Denmark*

A newly developed hypergeometric resummation technique [H. Mera *et al.*, Phys. Rev. Lett. **115**, 143001 (2015)] provides an easy-to-use recipe to obtain conserving approximations within the self-consistent nonequilibrium many-body perturbation theory. We demonstrate the usefulness of this technique by calculating the phonon-limited electronic current in a model of a single-molecule junction within the self-consistent Born approximation for the electron-phonon interacting system, where the perturbation expansion for the nonequilibrium Green's function in powers of the free bosonic propagator typically consists of a series of noncrossing sunset diagrams. Hypergeometric resummation preserves conservation laws and it is shown to provide substantial convergence acceleration relative to more standard approaches to self-consistency. This result strongly suggests that the convergence of the self-consistent sunset series is limited by a branch-cut singularity, which is accurately described by Gauss hypergeometric functions. Our results showcase an alternative approach to conservation laws and self-consistency where expectation values obtained from conserving divergent perturbation expansions are summed to their self-consistent value by analytic continuation functions able to mimic the convergence-limiting singularity structure.

I. INTRODUCTION

In contrast to bulk materials, nanostructures can be easily brought into far from equilibrium states by applying a bias voltage or external time-dependent fields [1]. Simulation tools [2–11] make it possible to evade usual trial-and-error experimental procedures by screening nanostructures *in silico* with desired properties for applications. The traditional semiclassical simulation tools cannot be used for quasiballistic nanometer-size active region attached to much larger reservoirs. On the other hand, accounting for all the relevant quantum many-body interactions for such systems composed of thousands of atoms is computationally prohibitively expensive [12,13]. For example, simulation of photocurrent in a photovoltaic cell requires us to take into account the electronic structure of the cell, electron-photon interactions responsible for photoexcitation, by electron-hole recombination processes, emission and absorption of phonons, and scattering by disorder [14]. Spintronic devices, such as spin-transfer torque magnetic random access memory [15], furnish another example of a complex quantum many-body system where electrons, magnons, and phonons interact with each other while being driven away from equilibrium [16–18].

The nonequilibrium Green's function formalism (NEGF) [2–4] provides a rigorous framework to model such systems by extending the many-body perturbation theory (MBPT) to out-of-equilibrium regimes. In the nonequilibrium steady state any one-particle observable can be calculated from the one-particle NEGF by solving the Dyson equation. In practice, however, the resulting equations need to be approximated. Typical approximations involve the use of finite-order perturbation theory (PT) [19–25], where the contour-ordered NEGF is approximated by a finite number of diagrams; or partial resummation schemes, such as the GW approximation [26–30], Where one class of diagrams (or a few of them) is summed to infinite order. Since there are infinitely many such classes, each containing an infinite number of diagrams, both finite-order PT and infinite-order resummation schemes are tentative at best. Furthermore, the NEGF equations and their approximations are nonlinear integral equations, which require a self-consistent solution [18,22], thus making their numerical solution very demanding from a computational perspective [13,21,23].

Nevertheless, both finite-order PT and infinite-order partial resummations are widely used to simulate out-of-equilibrium systems in the presence of interactions. The so-called self-consistent Born approximation (SCBA) [3] is a Hartree-Fock-like approximation commonly employed to model electron-electron, electron-phonon, electron-photon, and electron-magnon interactions. The SCBA is the simplest self-consistent noncrossing approximation that is also Φ derivable and, therefore, conserving [3]. Despite its simplicity, atomistic simulations using the SCBA can be very challenging, particularly when realistic system sizes are considered and a thorough exploration of the space of device parameters is intended [12,13,21,31–33]. Note that instances of unphysical convergence of self-consistent Φ-derivable approximations have been reported in recent literature [34–39].

Explicitly time-dependent systems pose an even more demanding challenge than steady-state ones. Time-dependent problems are typically approached by means of self-consistent Φ-derivable self-energy approximations within the Keldysh-Kadanoff-Baym equations (KBEs). Great progress has been made recently towards the application of KBEs to realistic stationary and time-dependent systems [40–48]. Interestingly, for very small systems under strong driving fields, unphysical behavior of self-consistent solutions from Φ-derivable approximations have been also reported in this context [42,43,48]. It should be added that the KBE approach has also been shown to be useful for the description of stationary systems [44,45].

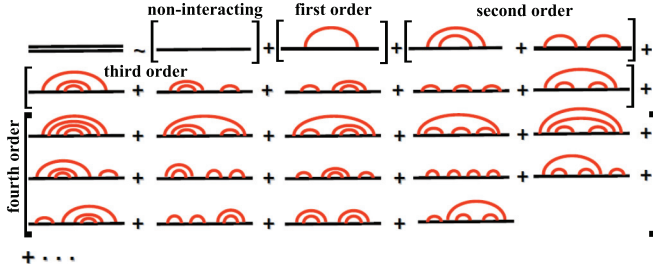*Corresponding author: hypergeometric2f1@gmail.com

FIG. 1. Diagrammatic representation of the interacting NEGF (double straight line) within the Fock-SCBA. This NEGF is asymptotic to a series in powers of the noninteracting NEGF (single straight line) and the boson propagator (semicircle). The brackets enclose all sunset diagrams contributing to each order in the expansion in powers of U^2 (square of the strength of electron-boson interaction).

Newly developed diagrammatic quantum Monte Carlo approaches [49–51] are able to deliver exact time-dependent perturbation expansions for expectation values; such expansions are typically divergent and therefore, in practice, need to be combined with a low-order resummation technique—the computation of large orders of PT being prohibitively expensive.

The purpose of this study is to demonstrate an alternative theoretical and computational approach where excellent approximations to the self-consistent results are obtained by combining finite-order PT with a recently developed hypergeometric resummation scheme [52–54]. For the sake of simplicity, we will use the Fock-only SCBA (Fock-SCBA) as a prototype of self-consistent partial resummation approximation, which, as illustrated in Fig. 1, consists of a series of self-consistent sunset diagrams. Nevertheless, we expect our insights to be useful for the calculation of quantities under other more involved—but equally uncontrolled—self-consistent resummation schemes [26–29]. While PT *per se* is at best an intrinsically weakly interacting approach, its combination with a carefully crafted analytic continuation function (ACF) can yield accurate results far beyond the weakly interacting limit, even allowing the calculation of intrinsically nonperturbative quantities from low-order PT [52–55].

For this purpose, hypergeometric functions $_pF_q$ are good candidates for ACF since they can mimic various types of singularities responsible for the divergence of a perturbation expansion. Thus far, hypergeometric resummation has only been applied to a handful of problems—originally it was tested using $_2F_1$ on the examples of divergent perturbation series in single-particle quantum mechanics [52,53]. The same approach was subsequently utilized for the calculation of field-assisted ionization in transition metal dichalcogenides [54] as well as in Ref. [55] for the calculation of the critical exponents in the two-dimensional Bose-Hubbard model—where higher-order hypergeometric functions $_pF_q$ were also considered. In these cases hypergeometric resummation revealed itself as a method superior to widely used resummation approaches, such as Shanks transformation [56], Padé approximants [57], and Borel-Padé resummation [56].

Here we demonstrate that hypergeometric resummation can be used to substantially simplify the calculation of expectation values from the self-consistent solution of the Dyson equation

in steady-state nonequilibrium MBPT. It will be argued by example that, relative to standard solvers for the Dyson equation in steady-state nonequilibrium MBPT, hypergeometric resummation has great potential to drastically reduce the computational cost of calculations without significantly impacting their accuracy.

The rest of the paper is organized as follows. In Sec. II, we give an overview of the standard approach to solve the Dyson equation self-consistently. Section III discusses perturbative approximations to the NEGF and Padé approximants as ACFs. In Sec. IV, we review the hypergeometric approximants from Ref. [52] and we introduce a new flavor of hypergeometric resummation based on the ratio test for series convergence. Section V introduces a physically motivated model of a single-molecule junction to which we apply various techniques discussed in previous sections by calculating the phonon-limited electronic current. A comparison with both Padé approximants and standard iterators reveals that hypergeometric resummation outperforms both of these approaches. In Sec. VI we discuss these results and argue that the self-consistent sunset series has a generally finite—but possibly very small—radius of convergence and that its divergence is due to a branch cut in an abstract plane of complex values for the electron-phonon interaction strength parameter. We conclude in Sec. VII.

II. SELF-CONSISTENT DYSON EQUATION

The central objects [2–4] of NEGF formalism are the one-particle contour-ordered GF, G, and self-energy $\Sigma = \Sigma[G]$. The latter is a functional of G that takes into account the effect of interactions and, in practice, needs to be approximated. G and $\Sigma[G]$ are related by the self-consistent Dyson equation

$$G = g + g\Sigma[G]G, \qquad (1)$$

which is a shorthand notation for

$$G(1,2) = g(1,2) + \int d3\,d4\, g(1,3)\Sigma(3,4)G(4,2). \qquad (2)$$

Here g is the noninteracting contour-ordered NEGF and $i = (\sigma_i, \mathbf{r}_i, t_i)$ is a global index encompassing spin, position, and time. The time arguments are located on the Keldysh-Schwinger contour, consisting of two counterpropagating copies of the real-time axis (the forward branch extending from $-\infty$ to ∞ and the backward branch extending from ∞ to $-\infty$), which is the hallmark of the NEGF formalism. Using the shorthand notation, we can also rewrite Eq. (1) as

$$G = [g^{-1} - \Sigma[G]]^{-1}. \qquad (3)$$

The Dyson equation must be solved for G and is explicitly self-consistent, thereby calling for an iterative scheme. The standard iteration proceeds as follows: one approximates $G \approx g$ and calculates $\Sigma[g]$ to build a new approximation $G_1 = [g^{-1} - \Sigma[g]]^{-1}$, then one approximates $G \approx G_1$ and evaluates $\Sigma[G_1]$. This procedure is then repeated typically according to the expression

$$G_n = [g^{-1} - \Sigma[G_{n-1}]]^{-1}, \qquad (4)$$

until G_n and G_{n-1} (or the relevant expectation values calculated from them) differ by less than some prescribed tolerance. This iterative procedure does not guarantee

convergence and often requires convergence acceleration schemes, such as linear and Pulay mixing, which typically need to be carefully combined with a preconditioning scheme such as Nieminen-Kerker [58,59] or direct inversion of the iterative subspace [60] without, again, guaranteeing convergence.

The appeal of self-consistent approaches over simpler forms of PT (to be discussed below) is based on the relationship between conservation laws and self-consistency [3,23,61]—it is well known that by choosing a conserving self-energy approximation, the expectation values calculated from the self-consistent G will obey whatever conservation laws they ought to obey, i.e., the fully self-consistent G is a conserving GF. However, as pointed out by Baym, [61,62] full self-consistency is by no means a necessary condition for conservation laws to be obeyed—a perturbation expansion in powers of the interaction strength will also be conserving at each and every order, provided that one chooses a conserving self-energy and keeps all the resulting terms at each order [22,23].[1] In contrast, an approximation such as G_1 obtained by setting $n = 1$ in Eq. (4) above is therefore not conserving because it misses some of the second-order diagrams owing to the fact that the perturbative expansion for the NEGF is not a geometric series [as incorrectly assumed in Eq. (4)]. While conserving, perturbative approximations are valid only for weakly interacting systems and break down very rapidly as the interaction approaches the radius of convergence of the perturbative expansion [56]. Thus, being conserving is not a good enough reason to choose an approximation for Σ. On the other hand, as we will demonstrate, being perturbative is not a good enough reason to discard an approximation.

In fact, critically reflecting on the basis of self-consistent approximations in MBPT is likely to raise some tough questions: it appears that the limit of validity of this method is identical to that of the underlying perturbation series. The reason for this is the neglect of—or the need to approximate—vertex corrections [28–30], which are present already at the second order in PT in the form of a first-order vertex. If one measures the accuracy of an approximation by the fraction of Feynman diagrams it accounts for, one readily sees that at high orders essentially all the Feynman diagrams include high-order vertex diagrams [63,64]. In practice, any form of self-consistent PT is an infinite-order approximation where, by including a finite-order approximation to the vertex, one is summing an error to infinite order [23,65]. But Σ is supposed to correct g—if the error is not small compared to the correction then self-consistent MBPT is not applicable; if it is small then a finite-order, perturbative approach is likely to be equally applicable. Accordingly, we see no fundamental reason for self-consistent MBPT to be favored over simpler forms of PT—if it works its perturbation series will, most likely, also work [22,23]. Also, very recent studies have shown that self-consistent Φ-derivable approximations can converge to unphysical solutions [34–43,46,47]; similar issues have been noted in the context of time-dependent simulations [40–43,46–48] using the Kadanoff-Baym equations, but can

be remedied by introducing self-consistent contributions in controlled fashion [42].

Nevertheless, the use of self-consistent MBPT may be justified to some extent. When a convergent self-consistent approximation is obtained it is typically regularized, i.e., it is free from the unphysically large values that one obtains from finite-order PT outside its radius of convergence. There are also more mundane reasons—we would like to have as many approximations as possible in our toolbox. Analytic continuation and resummation techniques may be very helpful in this respect because, as shown below, they may provide substantial convergence acceleration relative to state-of-the-art self-consistent solvers, which are based on the combination of Eq. (4) with mixers and preconditioners. These considerations highlight the importance of developing alternative approaches to self-consistency and conservation laws in MBPT.

III. PERTURBATIVE NEGF AND PADÉ RESUMMATION

An alternative to Eq. (4) is to compute the perturbation series for the NEGF, which is conserving if Σ is a conserving approximation, and compute expectation values from it. This yields a perturbation expansion for the expectation value. The perturbation expansion for the expectation value can then be analytically continued as analytic continuation naturally preserves the conservation laws.

Let us begin by considering an interacting many electron system, where the interaction is mediated by the exchange of bosons and described by the usual Feynman diagrams. To each vertex at the edges of a bosonic propagator we ascribe a parameter U, which controls the interaction strength. The perturbation expansion of G in powers of U^2 up to order N is then given by

$$g_N = g + \sum_{n=1}^{N} \delta g_n U^{2n}, \tag{5}$$

where δg_i are the expansion coefficients that do not depend of U. Therefore, perturbative NEGFs are polynomials in U^2, as illustrated for Fock-SCBA in Fig. 1.

A simple expression for g_N in terms of Σ is

$$g_N = g_{N-1} + g \sum_{n=1}^{N} \Sigma_n \Delta g_{N-n}, \tag{6}$$

where $\Delta g_n = \delta g_n U^{2n}$, $\delta g_0 = g_0 = g$ and Σ_n contains all the (proper) self-energy diagrams with n bosonic lines. Furthermore if, like in the case of the SCBA, Σ is a linear functional of G then $\Sigma_n = \Sigma[\Delta g_{n-1}]$: in this case it is straightforward to iterate Eq. (6) a couple of times. For $n = 1$ we get $g_1 = g + g\Sigma_1 g = g + \Delta g_1$; for $n = 2$ we get $g_2 = g_1 + g\Sigma_1 \Delta g_1 + g\Sigma_2 g$, and so on. Clearly we are getting the full perturbative expansion—terms coming from self-consistency (such as $g\Sigma_1 \Delta g_1$) and terms coming from Φ derivability (like $g\Sigma_2 g$). Therefore, as discussed in Ref. [23], g_N is actually conserving, albeit not fully self-consistent. Indeed, g_n contains a finite number of diagrams, while the fully self-consistent G contains an infinite number of them. The diagrammatic representation of g_4 in Fock-SCBA is shown in Fig. 1.

---

[1]The generalized Kadanoff-Baym ansatz (GKBA) has recently been shown to provide an alternative route for avoiding full self-consistency while preserving conservation laws. See Ref. [42].

As pointed out above, one could now take the sequence of g_n apply to it some sequence transformation such as Padé or Shanks. Unfortunately, as G_1 demonstrates, that does not typically lead to conservation laws. Instead these transformations can indeed be used as analytic continuation formulas, but on the sequence of expectation values obtained from the sequence of g_n. We can view G_1 as the 0/1 Padé approximant to the NEGF whose perturbation expansion is in general an unphysical geometric series that breaks conservation laws—it misses, for instance, the $g\Sigma_2 g$ discussed above.

In NEGF theory, any one-electron expectation value, $\mathcal{O}$, is a functional of the NEGF, $\mathcal{O} = \mathcal{O}[G]$. One can then evaluate the expectation value of an observable using g_n obtained from Eq. (6), $\mathcal{O}[g_N]$, thus generating a perturbation series for the expectation value to order N

$$\mathcal{O}_N \equiv \mathcal{O}[g_N] = \sum_{n=0}^{N} \delta o_n U^{2n} = \mathcal{O}_0 + \sum_{n=1}^{N} \Delta\mathcal{O}_n. \quad (7)$$

Here $\delta o_n = \mathcal{O}[\delta g_n]$ are the expansion coefficients, $\Delta\mathcal{O}_n = \delta o_n U^n$ is the nth $-$ order correction to the noninteracting expectation value, and we are assuming that the expectation value is a linear functional of G. The Born series has a radius of convergence U_c. For $U < U_c$ one finds $\lim_{N\to\infty} \mathcal{O}_N \to \mathcal{O}[G]$, while for $U > U_c$ the sequence $\mathcal{O}_N$ never converges to $\mathcal{O}[G]$ as N increases. In fact, increasing N for $U > U_c$ will only make things worse—the calculated expectation value either grows without bound or oscillates wildly between large negative and positive numbers [56].

However, sequence transformations [66,67] such as the Padé technique can actually accelerate convergence. For instance, given $\mathcal{O}_1 = \mathcal{O}_0 + \Delta\mathcal{O}_1$ and $\mathcal{O}_2 = \mathcal{O}_1 + \Delta\mathcal{O}_2$, we can build the 1/1 Padé approximant

$$\mathcal{O}_{1/1} = \frac{\mathcal{O}_0 + (\Delta\mathcal{O}_1^2 - \mathcal{O}_0\Delta\mathcal{O}_2)/\Delta\mathcal{O}_1}{1 - \Delta\mathcal{O}_2/\Delta\mathcal{O}_1}, \quad (8)$$

as well as the 0/2 Padé approximant. If instead we have the sequence of expectation values up to $N = 4$, we can build, e.g., 2/2 Padé approximant, but the equation is too long to be written here.

It has been shown [23] that by building a Padé table of expectation values one can achieve substantial convergence acceleration relative to the standard technique of calculating the sequence of $\mathcal{O}[G_n]$. However, there are some clear limitations—Padé resummation approximates the exact expectation value by a rational functions of U. Furthermore, the denominator of a given Padé approximant may vanish for specific values of the device parameters, rendering the approximation unusable and requiring the computation of higher orders in the perturbation expansion.

Ultimately, the root cause of the divergence of a perturbation expansion is a singularity in an abstract plane [68–71] of complex values of U (the physical values are located on the real axis). Padé approximants are able to describe the case where the convergence-limiting singularities are poles. But the singularity structure could also be a branch cut (a dense line of poles), and in such cases Padé approximants lack the necessary analytic structure to describe the physical U dependence, thus converging very slowly with perturbation order. In problems where convergence is limited by a branch

cut, Padé approximants quite literally attempt to reconstruct the cut by putting poles next to each other [56]. Accordingly the Padé sequence should converge slowly, if at all, for those cases. Simple low-order approximants able to account for both branch cut and poles should be advantageous [52].

It should be noted that the use of a bare perturbation series to compute expectation values has proven to be free of the pathological convergence to unphysical solution in self-consistent Φ-derivable theories. Indeed a bare series similar to the one we consider in this work, Eq. (6), was shown to converge to the physical branch in the examples discussed in Ref. [35]. This gives us further confidence in the soundness of approaches based on combining Eq. (6) with a suitable resummation technique.

IV. HYPERGEOMETRIC RESUMMATION

The combination of MBPT and analytic continuation of the expectation values calculated from it is a very promising and not widely explored approach to the computation of nonequilibrium properties of quantum many-body systems. It is naturally conserving and may well be a better option than the more standard methods, based on Eq. (4). Unfortunately, in typical sequence transformations such as Shanks or Padé, one approximates the U dependence of the expectation value by a rational function of U. Therefore, it is highly advisable to develop resummation techniques able to deal with both rational and nonrational functions of U, as well as with both poles and branch cuts in the complex U plane.

Here we put forward hypergeometric functions, in particular Gauss $_2F_1$ hypergeometric function, as tools for analytic continuation of expectation values calculated from MBPT. There are various reasons for this particular choice of analytic continuation functions: they are flexible and very general, including many other functions (such as binomials, exponentials, square roots, Bessel functions, etc.) as particular cases; they are able to mimic both cuts and poles and, thus, can naturally model the two main types of convergence-limiting singularity structures; their Taylor expansions are known, allowing one to build hypergeometric approximants in a fashion akin to Padé approximants.

Here we discuss two possible approaches to hypergeometric resummation. We first describe the hypergeometric approximant put forth in Ref. [52], and then introduce an alternative approach based on the ratio test of series convergence. In the first case, we seek approximations of the form

$$\mathcal{O} = {}_2F_1(h_1, h_2, h_3, h_4 U^2)\mathcal{O}_0, \quad (9)$$

while in the second case, one is lead to approximations of the form

$$\mathcal{O} = \mathcal{O}_0 + {}_2F_1(1, h_2', h_3', h_4' U^2)\Delta\mathcal{O}_1. \quad (10)$$

Here h_i and h_i' parameters are to be determined from the perturbation coefficients for $\mathcal{O}$, in a way that is fashioned after Padé resummation, by equating order-by-order the Taylor series for the hypergeometric approximants with the perturbation expansion for the observable. Fixing the parameters of both of these hypergeometric approximants requires four orders of PT. Thus, in the former approach one needs to determine the coefficients h_{1-4}, while in the latter one needs the first-order

correction $\Delta\mathcal{O}_1$, as well as the next three corrections, $\Delta\mathcal{O}_{2-4}$, in order to determine h'_{2-4}.

A. Hypergeometric approximant

Let us commence by recalling the construction of the hypergeometric approximant in Ref. [52]. First, the perturbation series for the expectation value of the observable under consideration is normalized by dividing it by its unperturbed value

$$\mathcal{O}/\mathcal{O}_0 = 1 + o_1 U^2 + o_2 U^4 + \cdots, \tag{11}$$

where $o_n = \delta o_n / \mathcal{O}_0$. The Taylor series for $_2F_1$ is

$$_2F_1(h_1, h_2, h_3; h_4 U^2) = \sum_{n=0}^{\infty} \frac{(h_1)_n (h_2)_n}{n!(h_3)_n} h_4^n U^{2n}, \tag{12}$$

where $(h_i)_n = \Gamma(h_i + n)/\Gamma(h_i)$ is a so-called Pochhammer symbol, defined in terms of the Euler Γ function. To obtain the h_i that determine the hypergeometric approximant, one equates each order in the asymptotic series for $_2F_1$ with the corresponding term in the perturbation expansion for $\mathcal{O}$, resulting in a set of four (nonlinear) equations with four unknowns h_{1-4}

$$o_n = \frac{(h_1)_n (h_2)_n}{n!(h_3)_n} h_4^n, \quad 0 < n \leqslant 4. \tag{13}$$

Because the equations are nonlinear, multiple solutions are possible. In the numerical example given below, however, two solutions were found, corresponding to the same hypergeometric function (see also Ref. [52]). Once the h_i have been obtained one has a hypergeometric approximant of the form given by Eq. (9). The hypergeometric function plays the role of a U-dependent multiplicative factor, which modulates the noninteracting expectation value bringing it, hopefully, in close agreement with the interacting result.

B. Hypergeometric approximants from the ratio test

Another flavor of hypergeometric resummation is inspired by the ratio test of series convergence. A useful way to know in many instances whether a series converges or not is the ratio test—one just needs to look at the ratio between consecutive expansion coefficients in the perturbation series for the expectation value, $r(n) = \delta o_n / \delta o_{n-1}$. If the ratio goes to a finite constant as $n \to \infty$ then the radius of convergence is not zero.

Let us then assume the radius of convergence to be not zero and approximate the ratio $r(n)$ between consecutive coefficients by a rational function—a diagonal Padé approximant

$$r(n) \equiv \frac{\delta o_n}{\delta o_{n-1}} \approx \frac{p_0 + p_1 n + \cdots + p_N n^N}{1 + q_1 n + \cdots q_N n^N}. \tag{14}$$

Here the coefficients p_i and q_i are to be determined from PT by calculating $r(n)$ for $n = 1, \ldots, 2N$ and solving the resulting equations for p_i and q_i. Note that Eq. (14) is the defining property of the hypergeometric series that sums to $_{N+1}F_N$.

The simplest rational approximation that generally tends to a nonzero constant as $n \to \infty$ is the 1/1 Padé approximant.

When applied to the ratio $\delta o_n / \delta o_{n-1}$ the 1/1 Padé approximant yields the hypergeometric $_2F_1$. So, we approximate

$$r(n) = \frac{\delta o_n}{\delta o_{n-1}} \approx \frac{p_0 + p_1 n}{1 + q_1 n}, \tag{15}$$

where p_0, p_1 and q_1 are parameters left undetermined for the time being. This recursive equation can be solved to yield an analytic approximation for o_n,

$$\delta o_n \approx \delta o_1 \frac{(-p_1/q_1)^{n-1}(2 + p_0/p_1)_{n-1}}{(2 + 1/q_1)_{n-1}}, \tag{16}$$

in terms of the lowest-order expansion coefficient δo_1 and the parameters p_0, p_1, and q_1. Now consider the perturbation expansion for the expectation value to infinite order, $\mathcal{O}_\infty = \sum_{i=0}^{\infty} \delta o_i U^{2i}$. For $U < U_c$ one has $\mathcal{O}[G] = \mathcal{O}_\infty$ and, therefore, one can replace δo_i by the expression given in Eq. (16), and then sum the resulting series to obtain $\mathcal{O}[G] \approx \mathcal{O}_0 +_2 F_1(1, 2 + p_0/p_1; 2 + 1/q_1; p_1 U^2/q_1)\Delta\mathcal{O}_1$. Therefore, starting from a power-series representation valid only for $U < U_c$, we have found an alternative representation valid also when $U > U_c$

$$\mathcal{O}[G] \approx \mathcal{O}_0 + {}_2F_1(1, 2 + p_0/p_1; 2 + 1/q_1; p_1 U^2/q_1)\Delta\mathcal{O}_1. \tag{17}$$

To find the values of p_0, p_1 and q_1, however, we need to calculate $\delta o_2/\delta o_1, \delta o_3/\delta o_2$, and $\delta o_4/\delta o_3$ numerically by means of Eq. (6). Alternatively one can solve the full Dyson equation and find $\mathcal{O}[G]$ as a function of U for small U, and from this dependence one immediately extracts δo_i, δo_1, δo_2, and δo_3. In the latter case one can use available self-consistent solvers based on Eq. (4) to obtain the coefficients for the ACF, while in the former case one needs to implement Eq. (6).

Once δo_i are found from the perturbation series of the expectation value, one uses Eq. (15) to obtain

$$r(1) = \frac{\delta o_2}{\delta o_1} = \frac{p_0 + p_1}{1 + q_1}, \tag{18}$$

$$r(2) = \frac{\delta o_3}{\delta o_2} = \frac{p_0 + 2p_1}{1 + 2q_1}, \tag{19}$$

$$r(3) = \frac{\delta o_4}{\delta o_3} = \frac{p_0 + 3p_1}{1 + 3q_1}, \tag{20}$$

which can be solved to find p_0, p_1, and q_1. Note that this procedure can be extended—by increasing the order of the Padé approximant for the ratio—to generate a sequence of approximants involving higher-order hypergeometric functions. We emphasize that expectation values calculated using either of the two flavors of hypergeometric resummation will satisfy conservation laws they ought to satisfy on the proviso that a conserving approximation is chosen for Σ.

V. PHONON-LIMITED ELECTRONIC CURRENT IN MOLECULAR JUNCTIONS VIA HYPERGEOMETRIC RESUMMATION

In this section we illustrate the potential of hypergeometric resummation as a convergence accelerator for the self-consistent solution of Eq. (1). We consider current-voltage (I-V) characteristics of the model of a single-molecule junction in the presence of electron-phonon interactions, treated at the

level of Fock-SCBA. We use Eq. (6) to evaluate the Fock-SCBA Feynman diagrams up to fourth order shown in Fig. 1, then compute expectation values from the resulting perturbative NEGF, and finally apply hypergeometric resummation to find approximations to the fully self-consistent expectation values. In the calculations shown below, this approach results in a speed up of about one to two orders of magnitude relative to the standard SCBA iteration based on Eq. (4).

A. Molecular junction model

We wish to try hypergeometric resummation in a steady-state nonequilibrium regime for an electron-boson interacting model that is as simple as possible, while retaining sufficient physics for it to be nontrivial. For transparency of discussion, we focus on electrons interacting with phonons, but our analysis can be applied to electrons interacting with other types of boson quasiparticles such as magnons [18]. A schematic view of such model, describing a single-molecule junction where electrons interact with a single-phonon mode, is depicted in Fig. 2(a). The model includes multiple-phonon processes and has a built-in asymmetry, so that conservation laws are not guaranteed by symmetry.

We consider an isolated molecule whose noninteracting Hamiltonian in the basis of molecular orbitals is diagonal, with eigenenergies ϵ_i, $i = 1, \ldots, 8$, as given by $\hat{h}_0 = \sum_i \epsilon_i c_i^\dagger c_i$ where $c_i^\dagger$ (c_i) creates (annihilates) one electron in the molecular orbital i. The eigenenergies are assumed to be equally spaced, satisfying $\epsilon_{i+1} - \epsilon_i = \Delta$. The unit of energy is set by $\Delta/2 = 1$, and we use $\hbar = 1 = e$ for simplicity. The noninteracting Hamiltonian is a diagonal matrix in the basis of molecular orbitals, which is taken to be $\hat{h}_0 = \text{diag}(-7, -5, -3, -1, 1, 3, 5, 7)$. This Hamiltonian describes noninteracting central region within the NEGF approach [2,3].

The central region is attached to semi-infinite ideal (i.e., with no disorder or many-body interactions) left (L) and right (R) electrodes, which terminate into mascroscopic reservoirs at infinity where electrons are assumed to be thermalized

at chemical potential μ_L or μ_R, respectively. The L, R leads are accounted for by self-energies $\Sigma_{L,R}^r$. Here we chose a wide-band limit and assume that the coupling to the electrodes does not break the symmetry of the molecule, so that the L and R self-energies are diagonal matrices in the basis of molecular orbitals, $(\Sigma_{L/R}^r)_{i,j} = -i\gamma_{L/R}\delta_{i,j}/2$. We choose $\gamma_L = 0.08$ and $\gamma_R = 0.1$. Since $\Delta/\gamma_R = 20$, the broadening of the molecular orbital energies induced by tunneling in and out of the electrodes is much smaller than the separation between the energy levels. The current is driven through the junction by applying the electrochemical potential difference $\mu_L - \mu_R = V_b$. The bias voltage V_b is applied symmetrically to the electrodes, i.e., $\mu_L = V_b/2$ and $\mu_R = -V_b/2$.

The noninteracting NEGF g yields the usual lesser $g^<$, greater $g^>$, retarded g^r and advanced $g^a = (g^r)^\dagger$ GFs via the Langreth rules [2,3]. In steady-state transport regime, these GFs Fourier transformed to frequency are given by

$$g^{r,a}(\omega) = \left[\omega I - h_0 - \Sigma_C^{r,a}(\omega)\right]^{-1}, \quad (21)$$

$$g^{<,>}(\omega) = g^r(\omega)\Sigma_C^{<,>}(\omega)g^a(\omega), \quad (22)$$

where I is the identity matrix and $\Sigma_C^r(\omega) = \Sigma_L^r(\omega) + \Sigma_R^r(\omega)$.

From $g^{r,a}(\omega)$ and $g^{<,>}(\omega)$ we can calculate any one-electron expectation value. For example, the noninteracting electronic current flowing through the interface between lead $\alpha = L, R$ and the central region is given by

$$\mathcal{I}_\alpha[g] = \frac{1}{2\pi}\int d\omega\, \text{Tr}[\Sigma_\alpha^<(\omega)g^>(\omega) - \Sigma_\alpha^>(\omega)g^<(\omega)], \quad (23)$$

where $\Sigma_{L,R}^<(\omega) = -2if_{L,R}(\omega)\text{Im}\Sigma_{L,R}^r(\omega)$, $\Sigma_{L,R}^>(\omega) = 2i[1 - f_{L,R}(\omega)]\text{Im}\Sigma_{L,R}^r(\omega)$ and $f_{L,R}(\omega) = f(\omega - \mu_{L,R})$ is the Fermi function of macroscopic reservoirs. In the numerical calculations shown below we assume zero temperature $T = 0$, which enters through the Fermi (or Bose-Einstein for phonons) distribution function.
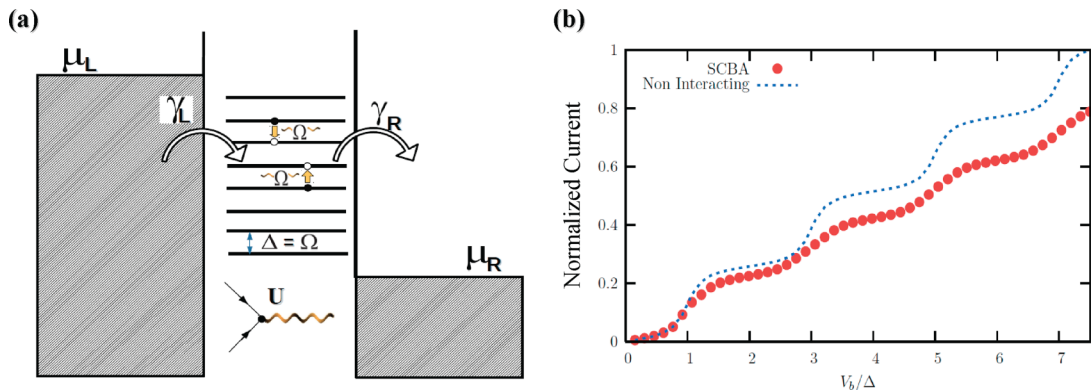

FIG. 2. Schematic view of the single-molecule junction model driven by finite bias voltage $\mu_L - \mu_R = V_b$. Here $\gamma_{L/R}$ is the tunneling rate in and out of the molecular electronic energy levels; Δ is the energy gap between neighboring levels; Ω is the phonon frequency of the single vibrational mode taken into account; and U is the strength of electron-phonon interaction. (b) Current-voltage characteristics of the single-molecule junction in (a) in the absence ($U = 0$, dashed line) and presence ($U = 4.0\gamma_R$, filled dots) of electron-phonon interaction. The latter case is computed using Fock-SCBA. The current is normalized by dividing by its noninteracting value at $V_b = 7.5\Delta$. For the model considered the interaction between electrons and phonon reduces the magnitude of the current relative to the noninteracting case.

B. Iterating the self-consistent Born approximation

The electron-phonon interaction is assumed to be localized in the central region. We consider only one free phonon mode of frequency $\Omega = \Delta$, i.e., resonant with the gap between molecular levels. This means that an electron in level i can make a transition to level $i \pm 1$ by emitting or absorbing a phonon. We assume that the phonons do not interact with each other and or flow into the electrodes, so they are described by the Hamiltonian $\hat{h}_{\text{ph}} = \Omega a^\dagger a$. Thus, electrons have no influence on the motion of phonons, but phonons are allowed to influence the electrons. The Hamiltonian describing electron-phonon interaction within the central region, which is added on $\hat{h}_0$, is given by

$$\hat{h}_{\text{int}} = \sum_{i,j} M_{i,j} c_j^\dagger c_i (a^\dagger + a), \qquad (24)$$

where $a^\dagger$ (a) creates (annihilates) one phonon in the central region. The matrix elements of the interaction matrix M are taken to be of the form $M_{i,j} = U \delta_{j,i\pm 1}$, where U is the interaction strength. Therefore phonon-induced electronic transitions are only between neighboring electronic levels.

The electron-phonon interaction effects out of equilibrium are most often treated at the SCBA level [12,21,34,72]. The SCBA can be further simplified to Fock-SCBA where noncrossing sunset-diagrams illustrated in Fig. 1 are retained while the Hartree diagrams are neglected [34]. In applications one also often neglects the real part of the electron-phonon Fock diagram [73]. These approximations work under the assumption of small polaron shifts. Here we adopt these additional approximations to simplify considerably numerical calculations while capturing essential features of inelastic electron-phonon scattering on the electronic current.

With these simplifications and approximations the lesser/greater and retarded self-energies that account for electron-phonon scattering within the electronic subsystem are given by

$$\Sigma_I^{<,>}(\omega) = M[(n_B(\Omega) + 1)G^{<,>}(\omega \pm \Omega) \\ + n_B(\Omega)G^{<,>}(\omega \mp \Omega)]M, \qquad (25)$$

$$\Sigma_I^r(\omega) = \tfrac{1}{2}[\Sigma_I^>(\omega) - \Sigma_I^<(\omega)], \qquad (26)$$

where $n_B(\Omega)$ is the Bose-Einstein distribution function and the top (bottom) signs in Eq. (25) correspond to the lesser (greater) self-energy. The retarded and lesser interacting NEGFs are given by

$$G^r(\omega) = [\omega I - \hat{h}_0 - \Sigma_C^r(\omega) - \Sigma_I^r(\omega)]^{-1}, \qquad (27)$$

$$G^<(\omega) = G^r(\omega)[\Sigma_C^<(\omega) + \Sigma_I^<(\omega)]G^a(\omega). \qquad (28)$$

The iterative solution of these equations is typically approached according to Eq. (4)—we start with $G \approx g$, evaluate $\Sigma_I^{<,>}$ and $\Sigma_I^r(\omega)$, calculate new $G^r(\omega)$ and $G^<(\omega)$, which are in turn used to evaluate a new approximation to $\Sigma_I^{<,>}(\omega)$ and $\Sigma_I^r(\omega)$.

The current in the interacting case is obtained also from Eq. (23) by replacing noninteracting $g^{<,>}$ with $G^{<,>}$. Because the SCBA is a conserving approximation the steady-state current is a conserved quantity, $\mathcal{I}_L[G] = -\mathcal{I}_R[G]$. We use

this fact as convergence criterion in the iteration of the SCBA equations, stopping the iteration when current conservation is violated by less than 0.001% in two consecutive iterations. One can verify that if $\gamma_L = \gamma_R$, current is automatically conserved as a result of the symmetry of the system. So to test current conservation it is necessary to choose $\gamma_L \neq \gamma_R$ in the calculations. We note that Eq. (4) leads to convergence issues already at low values of the interaction strength, independently of the convergence criterion. In order to speed up the convergence we proceed as follows: at each value of V_b we start from $U = 0$ and increase U slightly finding the self-consistent NEGF, which is then used as a starting point for a calculation with a slightly larger value than U. The procedure is repeated, slowly increasing U and using the self-consistent NEGF calculated from the previous value of U as a starting point, until we reach a self-consistent solution for $G^r(\omega)$ and $G^<(\omega)$ at the required large value U. When proceeding in this way we are able to converge SCBA calculations up to rather large values of $U \sim \Omega$. In contrast, using Eq. (4), convergence was problematic already for $U \sim \gamma_L$. Note that a very stringent convergence criterion was needed to obtain a self-consistent solution in full numerical agreement with the resummation results shown below.

The electronic current as a function of bias voltage V_b is shown in Fig. 2(b) for $U = 4\gamma_R = 0.4$. The inelastic electron-phonon scattering acts to reduce the current at large V_b by about 20% relative to its noninteracting value, while washing out the steps in the *I-V* characteristics of the noninteracting junction.

C. Perturbation series for the current

Instead of the conventional approach outlined in Sec. V B, one can use Eq. (6) to derive a conserving perturbation series for the current. This procedure requires $g_N^{<,>}$, which is obtained by applying Langreth rules

$$g_N^< = g_{N-1}^< + \left(g \sum_{n=1}^N \Sigma_n \Delta g_{N-n} \right)^< \qquad (29)$$

$$= g_{N-1}^< + g^r \sum_{n=1}^N \Sigma_n^< \Delta g_{N-n}^a$$

$$+ g^< \sum_{n=1}^N \Sigma_n^a \Delta g_{N-n}^a + g^r \sum_{n=1}^N \Sigma_n^r \Delta g_{N-n}^<. \qquad (30)$$

This means that $g_N^<$ can be written as

$$g_N^< = g^< + \Delta g_1^< + \cdots + \Delta g_N^<, \qquad (31)$$

where Δg_N is the Nth − order correction to g given by $g_N - g_{N-1}$, i.e., the sum of all the contributions containing N phonon lines, which is proportional to U^{2N}. Given that the current is a linear functional of G we can write

$$\mathcal{I}[g_N] = \mathcal{I}[g] + \mathcal{I}[\Delta g_1] + \cdots + \mathcal{I}[\Delta g_N] \qquad (32)$$

$$= \mathcal{I}_0 + \Delta \mathcal{I}_1 + \cdots + \Delta \mathcal{I}_N, \qquad (33)$$

which in the case studied here is the perturbation series for the current in SCBA.

D. High-bias current degradation

The high-bias current degradation is an important figure of merit in nanoelectronic devices [12]. It gives a metric for the impact of the various scattering mechanisms on the magnitude of electronic current. Here we quantify the high-bias current degradation using

$$\text{current degradation} = 100\left(1 - \frac{\mathcal{I}}{\mathcal{I}_0}\right), \qquad (34)$$

where both $\mathcal{I}$ and $\mathcal{I}_0$ are calculated in the high-bias regime that starts at $V_b/\Delta = 7.5$.

1. SCBA vs perturbation theory

In Fig. 3(a) we show the calculated values of the current degradation as a function of U, for $0 \leqslant U \leqslant 1$. The value $U = 1$ corresponds to $U/\gamma_R = 10$ and, therefore, cannot be considered a weak interaction. The current degradation is calculated by means of the standard SCBA iteration based on Eq. (4), as well as perturbatively by means of Eq. (6), using up to four orders of PT. The SCBA current degradation increases as a function of U, and reaches a value of about 35% for $U = 1$. We can see that perturbation theory does very poorly, oscillating wildly between odd and even orders. We observe that the perturbation expansion appears divergent outside of a small radius of convergence, $U_c \approx \gamma_L$ (note that $\gamma_L < \gamma_R$). Thus, the perturbative SCBA approach is therefore useless—the expansion is divergent and the self-consistent result is reproduced only for sufficiently small $U < U_c$.

Figure 3(a) clearly illustrates the advantages of iterating the SCBA equations (4) over the perturbation expansion of Eq. (6)—the standard iteration is in essence a resummation of the perturbation expansion for the NEGF that yields finite, well-behaved, I-V characteristics and current degradation in the presence of electron-phonon scattering. On the other hand Fig. 3(b) shows the potential problems with Eq. (4), which actually converges very slowly for $U > U_c$. As discussed in Sec. V B, at each value of U we input the self-consistent NEGF obtained from the previous value of U, which is slightly smaller, and yet some tens of iterations are typically needed to reach self-consistency, e.g., to converge the NEGF for $U = 0.2$ we start from the self-consistent solution obtained from $U = 0.19$ and need more than 10 iterations.

2. Hypergeometric resummation

One can conclude that Eq. (4) is not the most optimal choice to calculate expectation values from self-consistent MBPT. In Ref. [23] it has been shown that a combination of MBPT with Padé resummation can provide convergence acceleration relative to the standard SCBA iteration. In this section, we demonstrate that for the example considered in Fig. 2 hypergeometric resummation provides near-ultimate convergence acceleration, outperforming both the standard SCBA approach and Padé resummation.

In Fig. 4 we show the current degradation calculated as a function of U using both flavours of hypergeometric resummation introduced in Sec. IV A, which are obtained from fourth-order PT. Also shown are data obtained from the 1/1 and 2/2 Padé approximants. Hypergeometric resummation essentially reproduces the fully self-consistent result, all the
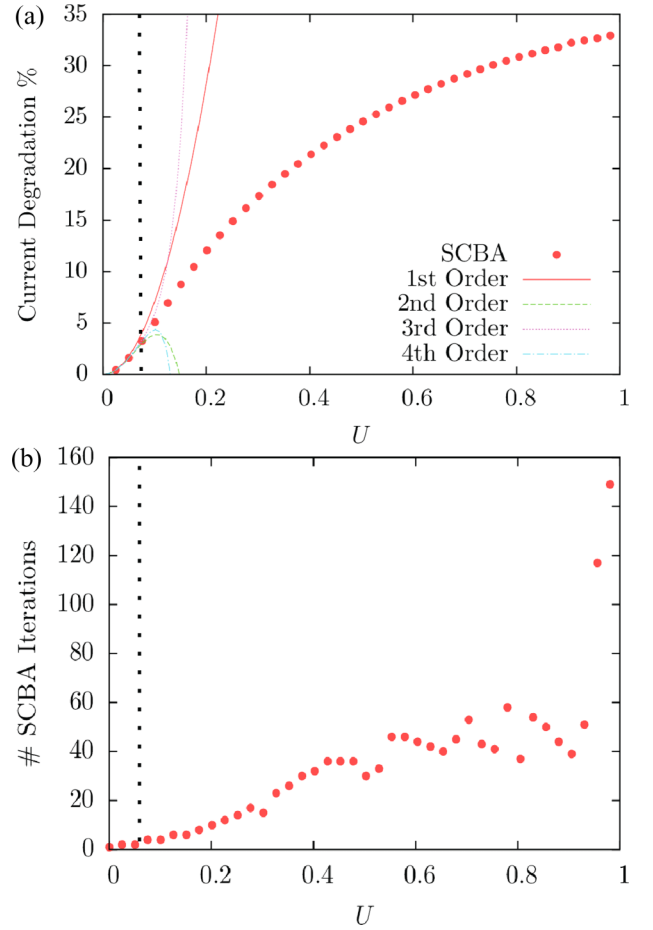

FIG. 3. (a) Phonon-induced degradation of the electronic current as a function of the electron-phonon interaction strength U, calculated within the standard Fock-SCBA (dots) or perturbative Fock-SCBA (thin lines). Perturbation theory reproduces the self-consistent result only for very weak interactions as it diverges for $U > U_c \approx \gamma_L$. The perturbatively calculated current degradation is unphysical because it oscillates wildly as higher-order corrections are added to the series. In contrast, the standard Fock-SCBA approach based on Eq. (4) yields a regularized converged result. (b) Number of iterations of Eq. (4) needed to converge the Fock-SCBA current. The vertical dotted black lines in both panels indicate the apparent radius of convergence, $U_c \approx \gamma_L$, of the perturbation series for electronic current. The bias voltage is set as $V_b = 7.5\Delta$.

way up to $U = 10\gamma_R = 1$, and outperforms the second-order (1/1) and fourth-order (2/2) diagonal Padé approximants. It is quite remarkable how hypergeometric resummation manages to transform the fourth-order PT result shown in Fig. 3(a) into the self-consistent result. The diagonal Padé approximants also appear to work rather well, but they substantially underestimate the current degradation. These results, together with those of Ref. [52], suggest that hypergeometric resummation is potentially a more powerful method than widely used Padé approximants to sum a divergent PT using only a few terms.

The hypergeometric resummation provides excellent approximations to the fully self-consistent result, but at a minute fraction of the computational cost required [13,21] by standard SCBA. For instance, using Eq. (4) about thousands of iterations are required to obtain the self-consistent result at $U = 1$, while
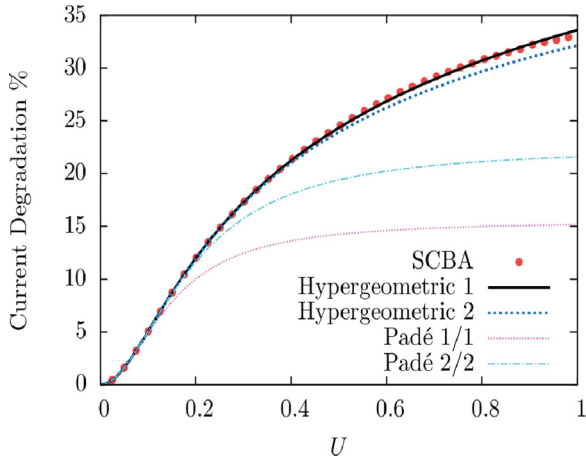
FIG. 4. Phonon-induced current degradation as a function of U calculated by the standard SCBA iteration given by: Eq. (4) (dots); the hypergeometric approximant given by Eq. (9) (thick solid line); the hypergeometric approximant given by Eq. (17) (thick dotted line); the 1/1 Padé approximant (thin dotted line); and the 2/2 Padé approximant (thin dot-dashed line). For the range of values of U considered both hypergeometric approximants give excellent approximations to the self-consistent result, as well as a substantial improvement over Padé approximants. The bias voltage is set as $V_b = 7.5\Delta$.

FIG. 5. *I-V* characteristics calculated by hypergeometric resummation (thick solid and dashed lines) is compared with standard Fock-SCBA (dots). For reference, we give also the noninteracting current (thin dashed line). The current has been normalized to its noninteracting value at $V_b = 7.5\Delta$. The value of the interaction strength is $U/\gamma_R = 4$. The hypergeometric estimates were obtained in just 54 iterations of Eq. (6)—a dramatic reduction relative to standard Eq. (4).

only four iterations of Eq. (6) are required to build both hypergeometric approximants. Importantly, both hypergeometric and Padé approximants are exactly conserving, while in the standard SCBA conservation laws are never exactly obeyed due to the finite tolerances of practical calculations. It is worth emphasizing that speed-up factors are highly dependent on the approach followed to iterate Eq. (4). However, given their magnitude it appears unlikely that an approach based on Eq. (4) could do better than hypergeometric resummation for the examples considered here.

We would like to emphasize that we have achieved identical results for the SCBA current degradation using two independent approaches, albeit with very different computational costs. On the one hand, we have used a bare perturbation expansion for the NEGF to evaluate the current in a very economical way; on the other hand, we have used the standard Eq. (4), together with a strategy based on increasing U slowly and a stringent convergence criterion, to obtain identical results but a much greater computational cost. Since Ref. [35] shows that the bare expansion converges to physical solution, we expect that the electronic currents computed by either of these two approaches are physical.

3. *I-V characteristics by hypergeometric resummation at high-bias voltage*

Finally, we turn our attention to the evaluation of the *I-V* characteristics in the presence of electron-phonon scattering for the single-molecule junction model in Fig. 2. In general the hypergeometric parameters of both approximants depend on the bias voltage V_b. Therefore, one needs to perform a fourth-order calculation for each value of V_b. However, in our calculations we note that the hypergeometric parameters
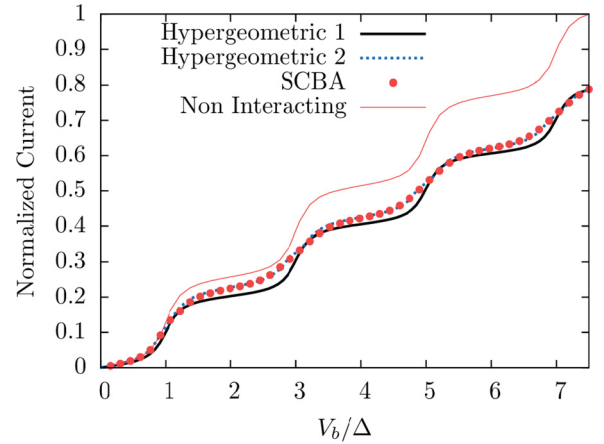
depend weakly on the applied V_b. This can be exploited to provide a very economical and accurate first-order approximation to the electronic current in Fock-SCBA. To do this, we determine the hypergeometric parameters at high V_b and assume that all bias voltage dependence is contained in the noninteracting current or the first-order current, depending on the hypergeometric approximant considered.

For this purpose, we use Eq. (9) to obtain

$$\mathcal{I}(V_b) \approx {}_2F_1(h_1, h_2; h_3; h_4 U^2)\mathcal{I}_0(V_b), \qquad (35)$$

or we use Eq. (17) to obtain

$$\mathcal{I}(V_b) \approx \mathcal{I}_0(V_b) + F(U)\Delta\mathcal{I}_1(V_b). \qquad (36)$$

Here $F(U) = {}_2F_1(1, 2 + p_0/p_1; 2 + 1/q_1; p_1 U^2/q_1)$ and the coefficients h_i and p_0, p_1, and q_1 do not depend on the bias voltage V_b. Applying these approximations to the model with parameter $U/\gamma_R = 4$ yields the *I-V* curves shown in Fig. 5. The thin solid line gives the noninteracting *I-V* characteristics, with well-defined steps in the typical staircase profile for transport through multilevel molecules. The red dots give the Fock-SCBA results obtained by iterating Eq. (4). As the electron-phonon interaction strength, the current is degraded and the steps in the *I-V* staircase are washed out. The *I-V* curve eventually becomes a linear function at sufficiently large U.

The thick solid line show results obtained from the hypergeometric approximant in Eq. (35). We see that this hypergeometric approximant provides a very good estimate for the current, although the steps are sharper than their SCBA counterpart. That shows that the voltage dependence in the noninteracting current is not enough to describe the interaction-induced washing out of the steplike structure. In contrast, the hypergeometric approximant in Eq. (36) accounts better for this effect of electron-phonon interactions. The standard Fock-SCBA and hypergeometric 2 *I-V* curves in Fig. 5 are almost indistinguishable for moderate interaction

strengths. Increasing $U > 4\gamma_R$ (data not shown) leads to Fock-SCBA computed *I-V* curves becoming nearly linear, while both hypergeometric approximants still exhibit some steplike structure and continue to give excellent estimates of the SCBA current. Note that there are 50 points in the *I-V* characteristics shown in Fig. 5, which require thousands of iterations when using Eq. (4) and only 54 iterations when using Eq. (6).

VI. DISCUSSION

In this paper, we introduced an alternative approach to self-consistency and conservation laws for nonequilibrium electron-boson quantum-many body systems treated by the NEGF formalism. Results of example calculations reveal that hypergeometric resummation [52] is a very promising approach to the summation of divergent series in MBPT, such as the Fock-SCBA. This technique is computationally much more efficient than standard iterators or resummation based on widely used Padé approximants. In this section, we argue that perturbation expansion associated with Fock-SCBA has a possibly very small radius of convergence, and that the singularity structure responsible for the divergence of the perturbation expansion is a branch cut. This observation can be substantiated by means of Feynman diagram counting argument inspired by Ref. [74].

To understand hypergeometric resummation, it is useful to imagine that the electron-boson interaction strength U is a complex parameter with both real and imaginary parts. In our example the physical system under consideration is recovered along the real axis. So let us consider the Fock-SCBA current as a function of complex U, $\mathcal{I} = \mathcal{I}(U)$. The observation of a divergent perturbation expansions in Fig. 3(a) signifies the presence of a singularity in the complex U plane. The radius of convergence is given by the distance U_c from the origin ($U = 0$) to the nearest singularity in $\mathcal{I}(U)$. The perturbation expansion for $\mathcal{I}(U)$ converges inside a circle $|U| < |U_c|$ and

diverges in the annulus $|U| \geqslant |U_c|$, where U_c can be zero. The perturbation expansion is a polynomial that is unable to mimic the localized nature of a pole or a branch cut in the complex U plane.

Padé approximants are able to account for poles, but they are not well suited to mimic branch cuts, unless one computes them to very large order. In Padé resummation branch cuts are replaced by a string of poles. The higher the order of the Padé approximant, the larger the number of poles used for the description of the branch cut and infinitely many poles are needed to precisely reproduce a branch cut. In contrast Gauss $_2F_1$ hypergeometric functions have a built-in branch cut, as shown in Figs. 6(a) and 6(b), and are also able to model poles. Thus, the fact that hypergeometric resummation outperforms Padé approximants suggests that the function $\mathcal{I}(U)$ contains a branch cut.

In Fig. 6 we show the imaginary part of the current Im $[\mathcal{I}(U)]$ in the complex U plane, as given by both hypergeometric approximants and the 1/1 and 2/2 Padé approximants. Clearly the hypergeometric approximants have a branch cut along the imaginary-U axis, while the Padé approximants have poles along the imaginary axis. The imaginary part of the hypergeometric approximants changes its sign discontinuously across the imaginary-U axis. In contrast, Padé approximants do not have the ability to model the branch cut, but instead accumulate poles along the imaginary axis as more orders of perturbation theory are used. Therefore when the convergence-limiting singularity is a branch cut, Padé approximants require many more orders of perturbation theory to be as accurate as fourth-order hypergeometric resummation.

It should be noted that so far we have been able to infer the presence of the branch cut in $\mathcal{I}(U)$ *a posteriori* through comparison with the fully self-consistent solution. One naturally wonders whether it would be possible to infer the presence of the branch cut *a priori*. To see this we apply a counting argument, originally put forth in Ref. [74],
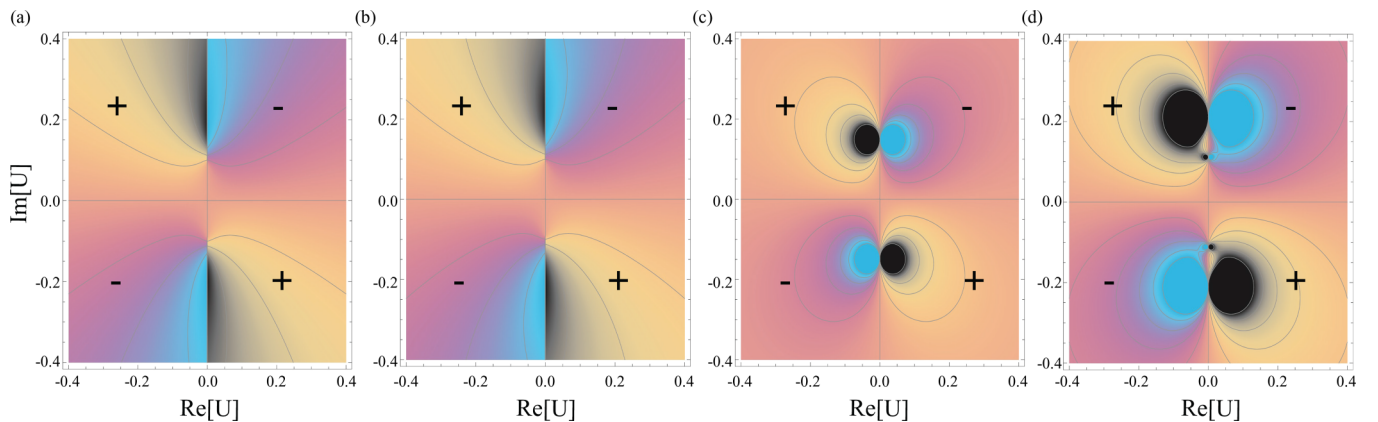

FIG. 6. Imaginary part of the phonon-limited electronic current at high bias voltage $V_b = 7.5\Delta$ in the model of single-molecule junction from Fig. 2 as a function of complex U. The sign of the imaginary part of the current on each quadrant is indicated by $\pm$. The physical current is found for Im $U = 0$ where the imaginary part of the current is zero. The current is calculated by summing the self-consistent sunset series in Fig. 1 by means of: (a) the hypergeometric approximant given by Eq. (9); (b) the hypergeometric approximant given by Eq. (17); (c) the 1/1 Padé approximant; (d) the 2/2 Padé approximant. In (a) and (b) the convergence-limiting singularity is a branch cut along Re $U = 0$; the imaginary part of the current discontinuously changes sign across the imaginary axis. In (c) and (d) the convergence limiting singularity is the closest pole to the origin. Padé approximants attempt to reproduce the cut by a line of poles—the 1/1 Padé approximant has two poles, while the 2/2 Padé approximant has four.

to the perturbation expansion of the self-consistent sunset diagrammatic series given by Eq. (6) and shown in Fig. 1, which lacks closed fermionic lines. Figure 1 shows that there is one first-order diagram, two second-order diagrams, five third-order diagrams, fourteen at fourth order, etc. The sequence 1, 1, 2, 5, 14, 42, 132, ..., is known as the Catalan sequence. The nth $-$ order self-consistent sunset series has C_n terms, where C_n is the nth $-$ order Catalan number. Consider then the series

$$\sum_{n=0} C_n x^n, \qquad (37)$$

which is known to be asymptotic to the generating function

$$\frac{2}{1 + \sqrt{1 - 4x}} = 1 + {}_2F_1(1, 3/2, 3, 4x)x,$$

that contains a square-root branch cut and has the same form as the hypergeometric approximant in Eq. (17) inspired by the ratio test of series convergence.

Hypergeometric approximants are very flexible functions able to adapt to both cuts and poles. This should be particularly true when the notion of hypergeometric resummation is understood broadly. Indeed, the reader may ask: Why ${}_2F_1$ and not $({}_2F_1)^{-1}$ or ${}_3F_2$? There are infinitely many hypergeometric approximants compatible with fourth-order data. These constitute an approximant space that needs to be carefully explored. Extra information might be needed to select an optimal approximant out of this space.

VII. CONCLUSIONS

In conclusion, we have applied a very recently developed hypergeometric resummation [52,53,55] to the calculation of physical observables in a nonequilibrium steady-state electron-boson quantum many-body system. In particular, we have considered the hypergeometric resummation of the noncrossing self-consistent sunset diagrammatic series (comprising Fock-SCBA) for the NEGF of electrons interacting with phonons in the presence of applied bias voltage, which can drive this system far from equilibrium. We tested the approach by computing the *I-V* characteristics and phonon-induced degradation of the electronic current at high-bias voltage applied to a model of single-molecule junction. Hypergeometric resummation of low orders of Fock-SCBA perturbation series for the current reproduces the full self-consistent solution at a fraction of the computational cost. The excellent performance of hypergeometric resummation strongly suggests the possibility that convergence of self-consistent sunset series is limited by branch-cut singularity. The development of more general resummation approaches for equilibrium and nonequilibrium MBPT, inspired by hypergeometric resummation considered here, and their deployment for realistic modeling of experimentally relevant systems constitutes a very interesting challenge, which we leave for future studies. In particular, it would be interesting to see whether new resummation procedures with tailored analytic structure can be of use in time-dependent problems. To this end it is clear that the combination of such resummation techniques with diagrammatic Monte Carlo (diagMC) techniques [51] offers the most direct route, as diagMC directly yields time-dependent perturbation expansions for the observables of interest.

[1] A. Kamenev, *Field Theory of Non-Equilibrium Systems* (Cambridge University Press, Cambridge, 2011).

[2] H. Haug and A.-P. Jauho, *Quantum Kinetics in Transport and Optics of Semiconductors* (Springer-Verlag, Berlin, 2008).

[3] G. Stefanucci and R. van Leeuwen, *Nonequilibrium Many-Body Theory of Quantum Systems: A Modern Introduction* (Cambridge University Press, Cambridge, 2013).

[4] K. Balzer and M. Bonitz, *Nonequilibrium Greens Functions Approach to Inhomogeneous Systems*, Lecture Notes in Physics, Vol. 867 (Springer, Heidelberg, 2013).

[5] M. Brandbyge, J. L. Mozos, P. Ordejón, J. Taylor, and K. Stokbro, Phys. Rev. B **65**, 165401 (2002).

[6] J. Taylor, H. Guo, and J. Wang, Phys. Rev. B **63**, 245407 (2001).

[7] J. J. Palacios, A. J. Pérez-Jiménez, E. Louis, E. SanFabián, and J. A. Vergés *et al.*, Phys. Rev. B **66**, 035322 (2002).

[8] D. A. Areshkin and B. K. Nikolić, Phys. Rev. B **81**, 155450 (2010).

[9] A. Pecchia and A. Di Carlo, Rep. Prog. Phys. **67**, 1497 (2004).

[10] R. Lake, G. Klimeck, R. C. Bowen, and D. Jovanovic, J. Appl. Phys. **81**, 7845 (1997).

[11] T. Kubis and P. Vogl, Phys. Rev. B **83**, 195304 (2011).

[12] R. Rhyner and M. Luisier, Phys. Rev. B **89**, 235311 (2014).

[13] M. Luisier, Chem. Soc. Rev. **43**, 4357 (2014).

[14] U. Aeberhard, Phys. Rev. B **86**, 115317 (2012).

[15] N. Locatelli, V. Cros, and J. Grollier, Nature Mater. **13**, 11 (2014).

[16] A. Manchon and S. Zhang, Phys. Rev. B **79**, 174401 (2009).

[17] P. M. Levy and A. Fert, Phys. Rev. B **74**, 224446 (2006).

[18] F. Mahfouzi and B. K. Nikolić, Phys. Rev. B **90**, 045115 (2014).

[19] J. K. Viljas, J. C. Cuevas, F. Pauly, and M. Häfner, Phys. Rev. B **72**, 245415 (2005).

[20] M. Paulsson, T. Frederiksen, and M. Brandbyge, Phys. Rev. B **72**, 201101 (2005).

[21] T. Frederiksen, M. Paulsson, M. Brandbyge, and A.-P. Jauho, Phys. Rev. B **75**, 205413 (2007).

[22] H. Mera, M. Lannoo, C. Li, N. Cavassilas, and M. Bescond, Phys. Rev. B **86**, 161404 (2012).

[23] H. Mera, M. Lannoo, N. Cavassilas, and M. Bescond, Phys. Rev. B **88**, 075147 (2013); See also Y. Lee, M. Lannoo, N. Cavassilas, M. Luisier, and M. Bescond, *ibid.* **93**, 205411 (2016).

[24] N. Cavassilas, M. Bescond, H. Mera, and M. Lannoo, App. Phys. Lett. **102**, 013508 (2013).

[25] M. Bescond, C. Li, H. Mera, N. Cavassilas, and M. Lannoo, J. App. Phys. **114**, 153712 (2013).

[26] K. S. Thygesen and A. Rubio, Phys. Rev. B **77**, 115333 (2008).

[27] C. D. Spataru, M. S. Hybertsen, S. G. Louie, and A. J. Millis, Phys. Rev. B **79**, 155110 (2009).

[28] L. K. Dash, H. Ness, and R. W. Godby, J. Chem. Phys. **132**, 104113 (2010).

[29] L. K. Dash, H. Ness, and R. W. Godby, Phys. Rev. B **84**, 085433 (2011).

[30] F. Tandetzky, J. K. Dewhurst, S. Sharma, and E. K. U. Gross, Phys. Rev. B **92**, 115125 (2015).

[31] T. Gunst, T. Markussen, K. Stokbro, and M. Brandbyge, Phys. Rev. B **93**, 245415 (2016)

[32] M. Calderara, S. Bruck, A. Pedersen, M. H. Bani-Hashemian, J. VandeVondele, and M. Luisier, *Proceedings of the International Conference for High Performance Computing, Networking, Storage and Analysis*, Article No. 3 (ACM New York, 2015).

[33] W. Zhang, C. Delerue, Y. M. Niquet, G. Allan, and E. Wang, Phys. Rev. B **82**, 115319 (2010); M. P. Persson, H. Mera, Y. M. Niquet, C. Delerue, and M. Diarra, *ibid.* **82**, 115318 (2010).

[34] W. Lee, N. Jean, and S. Sanvito, Phys. Rev. B **79**, 085120 (2009).

[35] E. Kozik, M. Ferrero, and A. Georges, Phys. Rev. Lett. **114**, 156402 (2015)

[36] R. Rossi and F. Werner, J. Phys. A **48**, 485202 (2015)

[37] A. Stan, P. Romaniello, S. Rigamonti, L. Reining, and J. A. Berger, New J. Phys. **17**, 093045 (2015); G. Lani, P. Romaniello, and L. Reining, *ibid.* **14**, 013056 (2012); J. A. Berger, P. Romaniello, F. Tandetzky, B. S. Mendoza, C. Brouder, and L. Reining, *ibid.* **16**, 113025 (2014).

[38] R. Rossi, F. Werner, N. Prokof'ev, and B. Svistunov, Phys. Rev. B **93**, 161102 (2016).

[39] T. Schäfer, S. Ciuchi, M. Wallerberger, P. Thunström, O. Gunnarsson, G. Sangiovanni, G. Rohringer, and A. Toschi, arXiv:1606.03393 (2016).

[40] N. Schlünzen, S. Hermanns, M. Bonitz, and C. Verdozzi, Phys. Rev. B **93**, 035107 (2016).

[41] M. Hopjan, D. Karlsson, S. Ydman, C. Verdozzi, and C-O. Almbladh, Phys. Rev. Lett. **116**, 236402 (2016).

[42] S. Hermanns, N. Schlünzen, and M. Bonitz, Phys. Rev. B **90**, 125111 (2014); S. Hermanns, K. Balzer, and M. Bonitz, J. Phys.: Conf. Ser. **427**, 012008 (2013).

[43] A. Stan, Phys. Rev. B **93**, 041103(R) (2016); N. Schlünzen and M. Bonitz, arXiv:1605.04588.

[44] K. Balzer, S. Bauch, and M. Bonitz, Phys. Rev. A **81**, 022510 (2010).

[45] N.-H. Kwong and M. Bonitz, Phys. Rev. Lett. **84**, 1768 (2000).

[46] E. Perfetto, A.-M. Uimonen, R. van Leeuwen, and G. Stefanucci, Phys. Rev. A **92**, 033419 (2015)

[47] S. Latini, E. Perfetto, A.-M. Uimonen, R. van Leeuwen, and G. Stefanucci, Phys. Rev. B **89**, 075306 (2014).

[48] M. Puig Von Friesen, C. Verdozzi, and C.-O. Almbladh, Phys. Rev. Lett. **103**, 176404 (2009).

[49] E. Burovski, E. Kozik, N. Prokofev, B. Svistunov, and M. Troyer, Phys. Rev. Lett. **101**, 090402 (2008).

[50] L. Pollet, N. V. Prokofev, and B. V. Svistunov, Phys. Rev. Lett. **105**, 210601 (2010).

[51] R. E. V. Profumo, C. Groth, L. Messio, O. Parcollet, and X. Waintal, Phys. Rev. B **91**, 245154 (2015).

[52] H. Mera, T. G. Pedersen, and B. K. Nikolić, Phys. Rev. Lett. **115**, 143001 (2015).

[53] T. G. Pedersen, H. Mera, and B. K. Nikolić, Phys. Rev. A **93**, 013409 (2016).

[54] T. G. Pedersen, S. Latini, K. S. Thygesen, H. Mera, and B. K. Nikolić, New J. Phys. **18**, 073043 (2016).

[55] S. Sanders, C. Heinisch, and M. Holthaus, Europhys. Lett. **111**, 20002 (2015).

[56] E. Caliceti *et al.*, Phys. Rep. **446**, 1 (2007).

[57] G. A. Baker and P. Graves-Morris, *Padé Approximants* (Cambridge University Press, Cambridge, 1996).

[58] R. M. Nieminen, J. Phys. F: Metal Phys. **7**, 375 (1977).

[59] G. P. Kerker, Phys. Rev. B **23**, 3082 (1981).

[60] G. Kresse and J. Furthmüller, Phys. Rev. B **54**, 11169 (1996).

[61] G. Baym, in *Progress in Nonequilibrium Green's Functions: Proceedings of the Conference Kadanoff-Baym Equations: Progress and Perspectives for Many-Body Physics Rostock, Germany, 20 24 September 1999*, edited by M. Bonitz (World Scientific, Singapore, 2000).

[62] G. Baym, Phys. Rev. **127**, 1391 (1962).

[63] L. G. Molinari, Phys. Rev. B **71**, 113102 (2005).

[64] L. G. Molinari and N. Manini, Eur. Phys. J. B **51**, 331 (2006).

[65] J. Gukelberger, L. Huang, and P. Werner, Phys. Rev. B **91**, 235114 (2015).

[66] E. J. Weniger, Comput. Phys. Rep. **10**, 189 (1989).

[67] E. J. Weniger, Appl. Numer. Math. **60**, 1429 (2010).

[68] F. J. Dyson, Phys. Rev. **85**, 631 (1952).

[69] A. Vainshtein, in *Continuous Advances in QCD 2002: ArkadyFest*, edited by K. Olive, M. Shifman, and M. Voloshin (World Scientific, Singapore, 2002).

[70] C. M. Bender and T. T. Wu, Phys. Rev. D **7**, 1620 (1973).

[71] I. M. Suslov, J. Exp. Theor. Phys. **100**, 1188 (2005).

[72] M. Luisier and G. Klimeck, Phys. Rev. B **80**, 155430 (2009).

[73] R. Valin, M. Aldegunde, A. Martinez, and J. R. Barker, J. Appl. Phys. **116**, 084507 (2014).

[74] C. M. Bender and T. T. Wu, Phys. Rev. Lett. **37**, 117 (1976).